Available online at www.sciencedirect.com
ScienceDirect
Journal of Catalysis 247 (2007) 101–111
JOURNAL OF CATALYSIS
www.elsevier.com/locate/jcat

Mechanistic study of the unusual catalytic properties of a new Ni–Ce mixed oxide for the CO_2 reforming of methane

Do Kyoung Kim [a,1], Klaus Stöwe [a], Frank Müller [b], Wilhelm F. Maier [a,*]

[a] *Lehrstuhl für Technische Chemie, Universität des Saarlandes, Gebäude C 4.2, 66123 Saarbrücken, Germany*
[b] *Institut für Experimentalphysik, Universität des Saarlandes, Gebäude C 6.3, 66123 Saarbrücken, Germany*

Received 27 October 2006; revised 16 January 2007; accepted 20 January 2007

Abstract

The origin of the exceptional properties of a $Ni_{10}Ce_{90}$ mixed oxide relative to a Ni/Al_2O_3 catalyst (i.e., immediate activity without catalyst prereduction, high resistance toward coking, high catalytic activity) and its catalytic deactivation for the CO_2 reforming of methane was investigated by XRD, XPS, pulse experimentation, and regeneration tests. Based on those results, a reaction mechanism is proposed. First, the catalytic property with no prereduction step relies on the reactivity of oxygen contained in the Ni phase. The rapid activation of $Ni_{10}Ce_{90}$ is based on the active interfacial oxygen in the Ni–Ce boundary, which leads to the complete oxidation of methane and the creation of active sites for the subsequent reforming reaction, whereas a slow decomposition of $NiAl_2O_4$ spinel results in a long induction period of the Ni/Al_2O_3 catalyst. Second, the coking resistance as well as the catalytic activity rely on the reactivity of lattice oxygen in the ceria. The ceria lattice oxygen participates in the reforming reaction through migration, which leads to the formation of oxygen vacancies. Subsequently, the vacancies are completely supplemented by oxygen arising from the dissociative adsorption of CO_2. Finally, the stability of $Ni_{10}Ce_{90}$ relies on the balance between the rate of generation and supplement of oxygen vacancies. Unbalanced rates of these processes result in deactivation.

Keywords: Methane reforming; CO_2; Ceria; Nickel catalysts; Ni–Ce interface; Autoactivation; Oxygen storage and release capacity (OSC); Pulse study; Sol–gel; Heterogeneous catalysis

1. Introduction

For applications of reforming catalysts in mobile fuel cells, high catalytic activity, no tendency toward coking, immediate catalyst startup, and long stability are desirable properties [1–3]. State-of-the-art Ni-catalysts, such as Ni on alumina, show a tendency for coking and deactivation and require a prereduction time to reach catalytic activity. The quest for alternative catalysts is difficult, because the possible number of compositions is almost infinite [4].

A previous study [3] used high-throughput synthesis and screening techniques in the search for and optimization of new autoactivation catalysts for the CO_2 reforming of methane. Although a large parameter space was sampled (more than 5000 mixed oxides containing 61 elements), no totally new catalyst was discovered. The study was conducted against a Rh/alumina reference catalyst, and rare noble metals were excluded. The best catalysts discovered were Ni-based mixed oxides; among these, a new $Ni_{10}Ce_{90}$ mixed oxide catalyst was identified that exhibits several unusual features: (1) lack of coking; (2) immediate activity (no need for prereduction), and (3) high catalytic activity. Continuous deactivation of the $Ni_{10}Ce_{90}$ catalyst could be strongly reduced by doping with 15 mol% Al or Zr. This is a significant improvement to a state-of-the-art Ni/Al_2O_3 catalyst, which tends to coke and deactivate and requires a prereduction step to reach the desired catalytic activity. Because of these unusual properties, it was of interest to investigate the nature of this ceria-based Ni catalyst in more detail.

Although cerium is one of the rare earth elements, the generic term "rare earth" can be misleading, because cerium is the 25th most abundant element in the earth's crust [5]. It

* Corresponding author.
E-mail address: w.f.maier@mx.uni-saarland.de (W.F. Maier).
[1] Current address: Department of Chemical Engineering, University of California, Berkeley, CA 94720, USA.

0021-9517/$ – see front matter
doi:10.1016/j.jcat.2007.01.011

is well known that in cerium oxide the elimination of lattice oxygen under reducing conditions leads to the creation of anionic vacancies (CeO_{2-x}) correlated to a high lattice oxygen mobility, and such oxygen vacancy defects are proposed to be the reactive sites on the surfaces of metal oxides [6]. Moreover, the nonstoichiometric CeO_{2-x} ($0 \leqslant x \leqslant 0.28$) easily restores its oxygen deficiency under oxidation conditions to form stoichiometric CeO_2 [7–9]. Recently, the structure, distribution, and formation of oxygen vacancies on a ceria surface were studied by means of scanning tunneling microscopy (STM) and density functional theory (DFT), and it was noted that the linear clusters of the surface oxygen vacancies formed on CeO_2 (111) expose exclusively Ce^{3+} ions to the gas-phase reactants [10]. Ceria is an important component of three-way catalysts in automobile applications, where it provides oxygen storage and release capacity (OSC) that enables control of the oxygen stoichiometry in the exhaust [7–9]. The same properties account for the exceptional properties of ceria-based oxides in various reactions, including steam reforming, hydrogenation, water–gas shift, and CO or hydrocarbon oxidation [7,11–15].

In the present study, the origin of the exceptional properties of a $Ni_{10}Ce_{90}$ mixed oxide relative to a Ni/Al_2O_3 catalyst (i.e., immediate activation in the absence of catalyst prereduction, high resistance toward coking, and high catalytic activity) and its catalytic deactivation for the CO_2 reforming of methane was investigated by XRD, XPS, pulse experiments, and regeneration tests.

2. Experimental

2.1. Catalyst preparation

The Ni_xCe_{100-x} ($x = 0, 10, 20, 100$) mixed oxides were prepared by the modified sol–gel method as described in detail previously [3]. The molar ratio of metal (1 M nitrate solution in methanol):complexing agent (4-hydroxy-4-methylpentanone):acid (propionic acid) was 100:300:2. For example, in the preparation of $Ni_{10}Ce_{90}$, 3.7 ml (30 mmol) of complexing agent was placed in a 100-ml glass beaker. Then 9.0 ml (9 mmol) of 1 M $Ce(NO_3)_3{\cdot}6H_2O$ solution in methanol and 1.0 ml (1 mmol) of 1 M $Ni(NO_3)_2{\cdot}6H_2O$ solution in methanol were added, and the resulting solution was magnetically stirred for 30 min, after which 15.0 μl (0.2 mmol) of propionic acid was added dropwise under continuous stirring. The solution was stirred for another 3 h while covered with Parafilm, to obtain a homogeneous solution. After the Parafilm was removed, the solution was transferred to a wide, shallow beaker and kept for 5 days at 40 °C for gelation. Then it was calcined in an oven at 65 °C for 5 h (at a heating rate of 0.2 °C min^{-1}) and at 250 °C for 5 h (at a heating rate of 0.2 °C min^{-1}). The catalyst powder thus obtained was manually ground in an agate mortar for 30 min, then recalcined in an oven, heated to 700 °C at a rate of 2 °C min^{-1}, and kept there for 2 h. Cerium oxide and nickel oxide were prepared by the same method. An artificial sample for XPS measurements was set by physical mixing of the nickel oxide and cerium oxide (the molar ratio of Ni:Ce = 1:9).

For comparison, a 10 mol% Ni-containing catalyst supported on commercial γ-Al_2O_3 (Johnson Matthey, S_{BET} = 255 $m^2\,g^{-1}$), designated Ni/Al_2O_3, was prepared by the wet-impregnation method as follows. After 1.268 g $Ni(NO_3)_2{\cdot}6H_2O$ in 10 ml water was stirred for 30 min in a flask, 2.0 g γ-Al_2O_3 was added into the solution. Then the mixture in the flask was stirred and evaporated at 50 °C in a rotary evaporator system (IKA Labortechnik). After the solvent was removed, the wet powder was dried in an oven at 120 °C for 24 h. The catalyst powder thus obtained was ball-milled for 30 min, then calcined in an oven, heated to 700 °C at a rate of 2 °C min^{-1}, and kept there for 2 h.

2.2. Reactivity testing of catalysts

Catalytic performance tests were carried out in a gas-phase quartz reactor (7 mm i.d., 400 mm long) at atmospheric pressure. Typically, 100 mg of the sample in fine-powder form (sieved fraction with 25–50 μm) was placed in the center of the reactor and held by quartz wool plugs. The reactor tube was heated inside an electric furnace. A quartz tube-sheathed K-type thermocouple was placed at the top of the catalyst bed to monitor the reaction temperature. The reactant gas [52.8 vol% CH_4 (quality 3.5) and 47.2 vol% CO_2 (4.8)], diluted with argon (5.0), was used without further purification. The following experimental conditions were typical for a single run. The catalyst was oxidized or reduced in situ at 600 °C for 2 h in flowing air or hydrogen (50 ml min^{-1}). After purging with Ar (50 ml min^{-1}) for 30 min, the gas flow was switched to an upstream reactant gas mixture ($CH_4/CO_2/Ar$ = 16.9/15.1/68; total flow, 65 ml min^{-1}). The gas hourly space velocity (GHSV) of each catalyst was calculated on the basis of the volume of the gas contacted with the catalyst per hour at standard conditions divided by the bulk volume of the catalyst particles. The volume of each catalyst was calculated as the ratio of the catalyst weight to its packed density determined before the experiments. The GHSV of $Ni_{10}Ce_{90}$ was 139,000 h^{-1}, and that of Ni/Al_2O_3 was 36,000 h^{-1}. The gas composition of products was analyzed by gas sensors (GfG-mbH) with ranges of 0–20 vol% CH_4, 0–25 vol% CO_2, and 0–10 vol% CO, along with a micro-gas chromatograph (model CP 4900, Varian). Each sample was tested for 10 h monitored with 60 GC measurements. A blank reaction test without catalyst was carried out to confirm that the reactor and thermocouple itself were not catalytically active.

For regeneration tests, the gas-phase composition over $Ni_{10}Ce_{90}$ was analyzed for 150 min by GC after every 10 min within a measurement run. After the reaction test, the catalyst was regenerated in situ at 600 °C for 2 h in a flow of air, Ar, or H_2 (50 ml min^{-1}). After purging with Ar (50 ml min^{-1}) for 30 min, the reaction test was conducted again. The regeneration cycle was performed once more.

2.3. Pulse experiment

The transient pulse experiments were performed in a gas-phase quartz reactor (3 mm i.d., 520 mm long) at atmospheric pressure. Typically, the sample in fine powder form (25–50 μm) was placed in the center of the reactor and held by quartz wool

plugs. The reactor tube was heated inside an electric furnace. The temperature of the catalyst bed was monitored by a thermocouple attached to the outside of the reactor tube. Before the pulse data were obtained, the catalyst was treated in situ at 600 °C for 150 min in flowing Ar (30 ml min^{-1}). During the pulse experiment, gas pulses [CH_4 (quality 3.5), CO_2 (4.8), or H_2 (5.0)] with a volume of 100 µl (ca. 4.07 µmol) were passed at 600 °C over the catalyst sample using Ar (5.0) as carrier gas (30 ml min^{-1}). The time between consecutive pulses was 5 min. The pulses of a different gas were introduced after stabilization for 30 min in flowing Ar (30 ml min^{-1}) at 600 °C. The products were monitored on-line by quadrupole mass spectrometry (QMS, GSD 300 T2, Balzers). The argon intensity of each pulse was chosen for internal standardization as representative within the chronological progress recording the detection sensitivity over the whole experiment. The normalized areas with respect to argon intensity under a peak were integrated, and then the integrated area was converted to a molar fraction, using a conversion factor determined after the experiments. The areas under the peaks were reproducible within about 8%. The conversion factors were determined under experimental conditions as close as possible to the product gas compositions in a blank reactor at 600 °C.

2.4. Catalyst characterization

Total BET surface areas were measured by nitrogen adsorption (Sorptomatic 1990, Carlo Erba) at the temperature of liquid nitrogen. The samples were outgassed overnight under vacuum at 200 °C before adsorption.

Temperature-programmed oxidation (TPO) was done by thermogravimetric analysis (TGA) using a Shimadzu TGA-50 thermogravimetric analyzer. After 10 h of reaction time, the catalyst sample was cooled to room temperature in a flow of Ar and then transferred to the TGA apparatus. About 50 mg of sample was loaded in a sample pan. The weight change of the catalyst was recorded in a flow of air (15 ml min^{-1}) as temperature was increased from room temperature to 900 °C at a rate of 15 °C min^{-1}.

The chemical composition of catalysts was analysed semiquantitatively by standardless X-ray fluorescence (XRF) spectroscopy (EAGLE II μ-Probe, EDAX) with RhK_α radiation using the fundamental parameter model. The X-ray beam was focused to a spot size of 300 µm on the sample surface.

Structural characterization of the $N_{10}Ce_{90}$ catalysts was performed by powder X-ray diffraction (XRD) with a Huber G 670 Guinier-camera using Cu$K_{\alpha 1}$ radiation ($\lambda = 1.54056$ Å). The powder diffraction patterns of the Ni/Al_2O_3 catalysts were recorded by a D5000 diffractometer (Bruker–Nonius Corp.) in focusing Bragg–Brentano reflection geometry with a Cu fine-focus tube ($U = 40$ kV, $I = 25$ mA) and a Johannson-type quartz monochromator [λ(Cu$K_{\alpha 1}$) = 1.54056 Å]. The diffracted intensity was measured by a linear position sensitive detector with Ar/10% methane filling at 8.5 bar pressure and an aperture of 10 mm to improve spatial resolution. In step-scan mode, the step width was ca. 0.015° in 2θ. Lattice parameter refinement was done by full-pattern Rietveld refinement with the program TOPAS [16] using the fundamental parameters approach [17].

Table 1
Catalytic behavior and coking rate on Ni/Al_2O_3 and $Ni_{10}Ce_{90}$ depending on the different pretreatments

Catalyst	Treatment[a]	Conversion (%)[b]				TGA[c] coke
		10 min		600 min		($g_C\ g_{cat}^{-1}\ h^{-1} \times 100$)
		CH_4	CO_2	CH_4	CO_2	
Ni/Al_2O_3	Oxidation	4.6	7.9	30.7[d]	36.9[d]	2.28
	Reduction	38.8	48.5	38.0	45.4	1.00
$Ni_{10}Ce_{90}$	Oxidation	32.3	48.7	27.6	38.3	0.08
	Reduction	6.2	15.2	4.9	6.6	0.01

[a] Pretreated in situ at 600 °C for 2 h in flowing air or hydrogen (50 ml min^{-1}).
[b] Operating conditions: $T = 600$ °C; $p = 1$ bar; total flow 65 ml min^{-1} ($CH_4/CO_2/Ar = 16.9/15.1/68$); catalyst weight $m = 0.100$ g.
[c] Operating conditions: catalyst weight $m \approx 0.050$ g; T increasing rate 15 °C min^{-1}; air total flow 15 ml min^{-1}.
[d] Measured after 380 min due to reactor clogging.

X-ray photoelectron spectra (XPS) were recorded by a VG ESCALAB MK II spectrometer using AlK_α radiation (1486.6 eV). The reaction or reduction of samples was performed in a gas-phase quartz reactor with an on/off valve on the top and bottom of the reactor. The reactor with the sample under Ar was transferred to a glove box, in which the sample in powder form was mixed with zirconium (about one-third of total weight) to compensate for charging of the nonconducting samples during the measurement, and pressed into a pellet. The resulting pellet was placed in a transfer chamber with a stainless steel sample holder under the inert conditions to avoid any exposure to the atmosphere before the analysis. The XPS data from the regions related to the C 1s, O 1s, Ce 3d, and Ni 2p core levels were recorded for each sample. The binding energies were adjusted relative to C 1s at 284.5 eV.

3. Results and discussion

3.1. Catalyst performance and carbon deposition

The chemical composition of each catalyst was verified by XRF. According to BET measurements of each material after calcination at 700 °C, fresh ceria (19.7 $m^2\ g^{-1}$), nickel oxide (29.4 $m^2\ g^{-1}$), and $Ni_{10}Ce_{90}$ mixed oxide (36.9 $m^2\ g^{-1}$) had a low surface area, and γ-Al_2O_3 (255.0 $m^2\ g^{-1}$) and Ni/Al_2O_3 (205.9 $m^2\ g^{-1}$) had a relatively high surface area.

Equilibrium conversions of CH_4 and CO_2, calculated by the equiTherm software [18], were 53.1 and 69.4%, respectively, with a H_2/CO ratio of 0.85 at 600 °C. Only at 800 °C the equilibrium conversions reached almost total consumption (87.8% CH_4 and 99.1% CO_2, respectively) with a H_2/CO ratio of unity. Catalytic activity tests of $Ni_{10}Ce_{90}$ and Ni/Al_2O_3 were performed for the CO_2 reforming of methane after in situ oxidation or reduction at the reaction temperature (600 °C). The reaction conditions (residence time, catalyst amount) were chosen to stay in the kinetic regime by keeping the conversion significantly below thermodynamic equilibrium.

Table 1 summarizes the catalytic performance and tendency toward coking on Ni/Al_2O_3 and $Ni_{10}Ce_{90}$ depending on the dif-

ferent pretreatments. The oxidized Ni/Al_2O_3 showed low initial activity that did not start to increase until after almost 80 min, with catalytic activity stabilizing only after about 240 min (long induction period) [3]. Moreover, Ni/Al_2O_3 led to reactor plugging after only 380 min due to strong carbon deposition (2.28 wt% h^{-1}) [3]. The prereduced Ni/Al_2O_3 revealed an immediate activity and relatively high rate of coke formation (1.00 wt% h^{-1}), although reactor plugging was not detected. For the Ni/Al_2O_3 catalyst, a prereduction step or long induction period was required to reach catalytic activity, and carbon deposition was favored regardless of the pretreatment conditions. In strong contrast, the oxidized $Ni_{10}Ce_{90}$ exhibited a rapid startup operation and high coking resistance (0.08 wt% h^{-1}) [3], whereas prereduced $Ni_{10}Ce_{90}$ demonstrated low activity and negligible tendency toward coking (0.01 wt% h^{-1}). The oxidized $Ni_{10}Ce_{90}$ was much more active than the reduced $Ni_{10}Ce_{90}$, and both samples showed high resistance to carbon deposition and a continuous decrease of conversions. Wang and Lu reported that in catalytic activity tests after prereduction, Ni/CeO_2 showed much lower activity and carbon deposition relative to Ni/Al_2O_3 [19], in agreement with our results, presented in Table 1.

The strong tendency toward carbon deposition of Ni/Al_2O_3 also could originate from compacting problems of the high-surface area Al_2O_3, leading to a pressure increase. But this possibility was excluded, because testing of 400 mg of $Ni_{10}Ce_{90}$ (GHSV 35,000 h^{-1}, with the same bed volume and particle size distribution as that of Ni/Al_2O_3) under identical conditions also demonstrated high coking resistance.

To elucidate the effect of treatment conditions (oxidation, reduction, or inertness) on the catalytic activity in more detail, we tested $Ni_{10}Ce_{90}$ catalysts with different sequences of regeneration procedures, as shown in Fig. 1. As shown in Fig. 1a, fresh $Ni_{10}Ce_{90}$ (after in situ oxidation) always exhibited an immediate high catalytic activity, which then slowly decreased. After about 150 min of reaction time, the catalyst was regenerated with air, in the other two experiments with Ar, and in the last with hydrogen; the regeneration time was always 30 min (not shown in Fig. 1). The CO_2-conversion results, depicted in Fig. 1b, also prove that the treatment with air led to full recovery of the initial activity. Deactivation continued after Ar treatment. H_2 treatment led to a dramatic reduction of catalytic activity.

After another 150 min of reaction time, the catalysts were regenerated again (see Figs. 1aC and 1bC). When the air-regenerated catalyst was regenerated with air again, most of its activity was recovered. The catalyst regenerated originally with Ar recovered most of its original activity after regeneration with air, whereas deactivation continued when it was regenerated again with Ar. The sample deactivated by the regeneration with hydrogen recovered only little of its original activity by the final air regeneration.

3.2. Characterization of Ni/Al_2O_3 catalyst

To see the effect of catalyst structure on the activity, XRD measurements were performed for the Ni/Al_2O_3 catalysts in as prepared state, after 2 h of reduction, and after 30 and 380 min

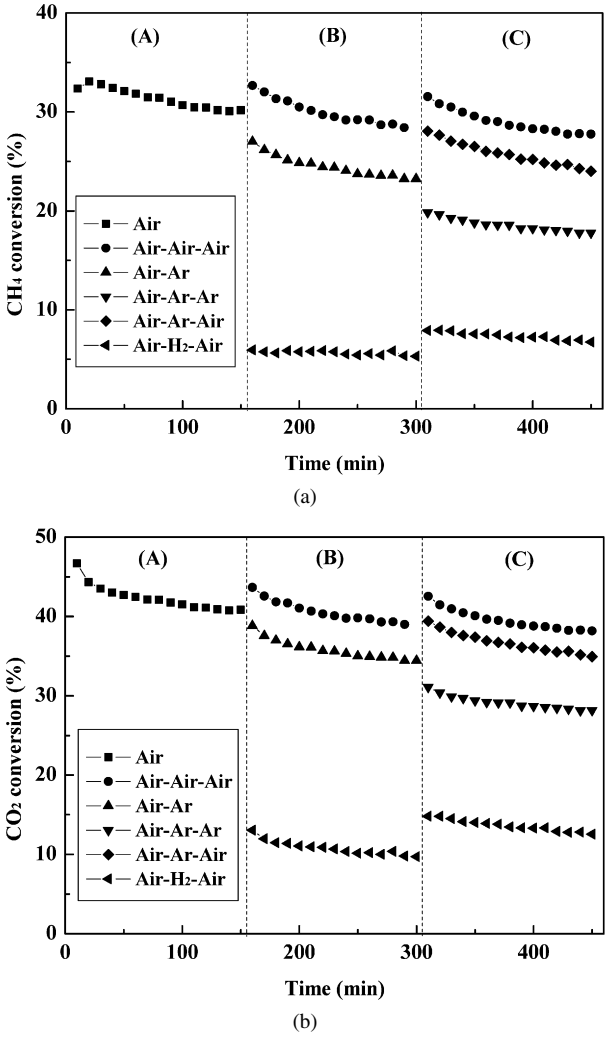

Fig. 1. Time dependence of the catalytic activity and stability of 100 mg $Ni_{10}Ce_{90}$ in a variety of regeneration conditions: (a) CH_4 conversion and (b) CO_2 conversion. Operating conditions: $T = 600\,^{\circ}C$; $P = 1$ bar; total flow 65 ml min^{-1} ($CH_4/CO_2/Ar = 16.9/15.1/68$). The different regeneration or pretreatment conditions are stated in the legend. (A), (B) and (C) indicate successive experiments.

of reaction. Fig. 2 shows the XRD pattern of as-prepared, reduced, and tested Ni on γ-Al_2O_3 in relation to that of the pure, undoped support. The XRD pattern of as-prepared Ni/Al_2O_3 shows main peaks at $2\theta = 37.3°$, 45.5°, and 65.3°, corresponding to the reflections (311), (400), and (440) of cubic Al_2O_3. The absence of reflections at $2\theta = 43.3°$ and 63.0° indicates that no NiO was formed in the Ni/Al_2O_3 catalyst. A possible reaction product of the wet-impregnation method is the spinel-phase $NiAl_2O_4$, which crystallizes isotypically to the γ-Al_2O_3 support in a fcc oxygen packing with partial occupation of voids. As a result of this structure relation, a solid solution between the two boundary phases is formed, which can be described by the formula $Ni_{3x}Al_{8-2x}O_{12}$ ($0 \leqslant x \leqslant 1$). Due to the very similar lattice dimensions, the composition of the product formed cannot be deduced from inspection of the diffraction pattern alone; thus, a Rietveld refinement of the complete diffraction pattern would seem to be advisable. On the other hand,

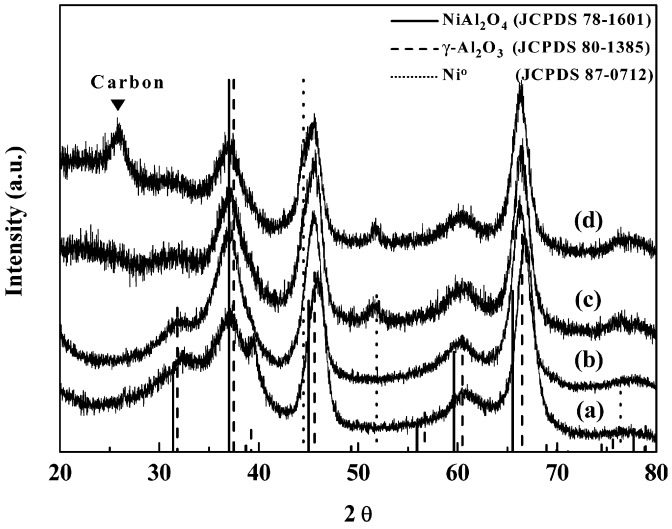

Fig. 2. XRD patterns of as prepared, reduced and tested Ni/Al_2O_3 relative to the fine γ-Al_2O_3 support: (a) γ-Al_2O_3, (b) as prepared Ni/Al_2O_3, (c) reduced Ni/Al_2O_3 (after 2 h reduction of sample (b)), and (d) tested Ni/Al_2O_3 (after 380 min reaction of sample (b)).

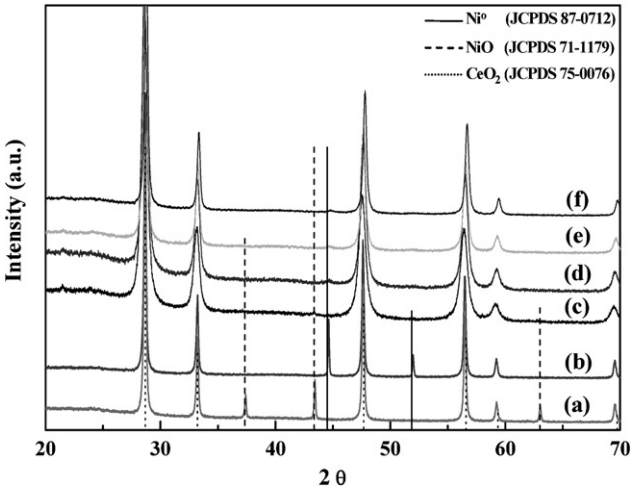

Fig. 3. XRD patterns (a) of the as prepared artificial sample (physical mixing of nickel oxide and cerium oxide both prepared by the sol–gel method, the molar ratio of Ni:Ce = 1:9); (b) after 2 h reduction of sample (a); (c) of as prepared $Ni_{10}Ce_{90}$; (d) after 10 h reaction of sample (c); (e) after 2 h reduction of sample (c); (f) after 10 h reaction of sample (e).

the diffraction patterns shown in Fig. 2 are characterized by very broad reflections due to the poor crystallinity and small crystallite size of the calcined reaction product, which affected all results from Rietveld refinements because of the low significance level of the refinement results. A major difference between the diffraction pattern of $NiAl_2O_4$ and γ-Al_2O_3 is the intensity of the (222) reflection at about $2\theta = 39.4°$ (compare Fig. 2, patterns a and b). Based on the low intensity of the (222) reflection in the diffraction pattern of the reaction product, we deduce a spinel formation according to the formula given above with undetermined Ni content in agreement with previous investigations [20].

For the reduced Ni/Al_2O_3 catalyst, a new peak at $2\theta = 51.8°$ as well as a line broadening at the lower angle side of the spinel (400) reflection at $2\theta = 45.5°$ is interpreted as formation of metallic nickel. Analysis of a diffraction pattern for the sample after the reaction of fresh catalyst revealed no significant change after 30 min of reaction (not shown) compared with the as-prepared Ni/Al_2O_3. After 380 min of reaction, the peak at $2\theta = 51.8°$ and line broadening at the lower angle side of the spinel (400) reflection at $2\theta = 45.5°$ were detectable similarly as in the reduced catalyst, and a very broad diffraction intensity was seen around $2\theta = 26.4°$, assigned to the formation of carbon. It is well known that carbon is readily deposited on the Ni/Al_2O_3 catalyst under our experimental conditions, as was demonstrated in the TPO study (see Table 1).

In catalytic testing, the oxidized Ni/Al_2O_3 maintained a low initial activity until almost 80 min. In the XRD pattern of the Ni/Al_2O_3 catalyst, the nickel in as-prepared state was present in the form of $NiAl_2O_4$ spinel, which maintained its state for at least 30 min of reaction. The Ni/Al_2O_3 catalyst reduced for 2 h or tested for about 240 min demonstrated high and stable catalytic conversions. Here the Ni oxidation state was Ni^0, which represents a presumably active center for the reforming reaction. Thus, the slow increase of conversion during the activation period is attributed to the continuous reduction of the $Ni_{3x}Al_{8-2x}O_{12}$ species by methane, which can be promoted by product gas (hydrogen) according to the following equation:

$$Ni_{3x}Al_{8-2x}O_{12} + 3xH_2 \rightarrow 3xNi + (4-x)Al_2O_3 + 3xH_2O.$$

XRD characterization of Ni/Al_2O_3 indicates a correlation between catalytic activity change and Ni oxidation state, and the long induction period of Ni/Al_2O_3 catalyst is due to a slow decomposition of $NiAl_2O_4$ spinel to metallic nickel and Al_2O_3.

Severe coke formation on the tested Ni/Al_2O_3 was supported by XRD (Fig. 2d) and TPO studies (see Table 1). Pulse experiments for nickel oxide (see Section 3.4) demonstrated that reduced nickel decomposes methane to H_2 and carbon, and the surface carbon on metallic nickel is not removed by CO_2. In addition, it is known that γ-Al_2O_3 is an irreducible support which does not provide lattice oxygen [21]. Thus, a lack of oxygen supplied from gas phase or catalyst support capable of eliminating the surface carbon on Ni^0 contributes to the high coking tendency of Ni/Al_2O_3.

3.3. Characterization of Ni–Ce mixed oxide

XRD measurements were performed for the $Ni_{10}Ce_{90}$ catalyst in its as-prepared state, after 2 h of reduction, and after 30 and 600 min of reaction (Fig. 3, patterns c–f). The patterns are dominated by the diffraction peaks of the ceria substrate, revealing a much lower peak-width FWHM, that is, a much better crystallinity and larger crystallite size compared with γ-Al_2O_3, but lower crystallinity than the pure oxide as prepared by the sol–gel method. The reflections of oxidized nickel (I_{100} at $2\theta = 43.4°$) and metallic nickel (I_{100} at $2\theta = 44.5°$) on the catalysts are very weak; this, along with the line broadening, indicate high dispersion of the Ni. The small metal particles and their high dispersion in $Ni_{10}Ce_{90}$ are attributed to an intrinsic result of the acid-catalyzed sol–gel preparation, which is known to provide atomically dispersed mixed oxides

[22,23]. Moreover, a linear decrease of the CeO_2 lattice parameter with increasing Ni amount was identified for the pure CeO_2 $a = 5.4135(1)$ Å, as-prepared $Ni_{10}Ce_{90}$ $a = 5.4124(3)$ Å, and $Ni_{20}Ce_{80}$ $a = 5.411(1)$ Å, which follows Vegard's law [24]. This suggests an oxide solid solution was formed in the Ni–Ce mixed oxide system with incorporation of some Ni^{2+} ions into the ceria lattice, in agreement with previous investigations [25,26]. Formation of the solid solution is attributed to the acid-catalyzed sol–gel process used for synthesis of the material. The lack of a carbon peak (at $2\theta = 26.4°$) in the XRD patterns of tested samples confirms the high coking resistivity of this $Ni_{10}Ce_{90}$ mixed oxide, which is consistent with the results of our TPO study (see Table 1).

A control experiment with identical composition (shown in Fig. 3, patterns a and b) found that metallic Ni and Ni oxide can be clearly identified when present as bulk materials. For fresh CeO_2 and NiO prepared by the sol–gel method, the XRD pattern revealed a fluorite-type structure [$a = 5.4135(1)$ Å] and a cubic rock-salt structure [$a = 4.1793(1)$ Å], respectively. These data were used as reference. The XRD patterns of the artificial sample (physical mixing of the nickel oxide and cerium oxide prepared by the sol–gel method, at a molar ratio of Ni:Ce = 1:9) in as-prepared and reduced state are shown in Fig. 3, patterns a and b. Clearly, the reflections of oxidized nickel (i.e., NiO [I_{100} at $2\theta = 43.4°$]), on the as-prepared sample and metallic nickel (I_{100} at $2\theta = 44.5°$) on the reduced sample are detectable, confirming the foregoing conclusions on the nature of the Ni in the mixed oxide.

XPS was used to obtain further information about the valency/oxidation state of elements and surface composition of the Ni–Ce mixed oxide by inspecting the spectral line shape and the intensities of the Ce 3d and Ni 2p core-level electrons. Due to the surface sensitivity of XPS, special precautions were taken to avoid contact of the samples with air during introduction into the XPS analysis chamber. In addition, the samples were mixed with zirconium to reduce charging of the nonconducting samples during the measurement, as described in Section 2. Despite the comparable photoemission cross-sections of Ce 3d and Ni 2p, the intensity of Ni 2p dropped below the nominal 10:90 ratio for the $Ni_{10}Ce_{90}$ catalysts; due to the very weak intensities, even a qualitative interpretation of the Ni 2p line shape was not possible. Even in the case of $Ni_{20}Ce_{80}$ catalysts with the higher Ni/Ce ratio, Ni 2p intensity was very weak. Fig. 4 compares the Ce 3d spectra of the $Ni_{20}Ce_{80}$ catalysts in as prepared state, after reduction for 2 h, and after reaction for 2 h with the Ce 3d spectra of Ce_2O_3 and CeO_2 [27,28]. According to literature data [25,29,30], the CeO_2 spectrum (representing Ce^{4+}) is labelled with v, v″, v‴ and u, u″, u‴, describing the $3d_{5/2}$ and $3d_{3/2}$ photoelectron intensities for $4f^2$, $4f^1$, and $4f^0$ occupation, and v′ and u′, representing the lower binding energy intensities of the $3d_{5/2}$ and $3d_{3/2}$ electrons for the $4f^1/4f^2$ configuration in Ce_2O_3 (representing Ce^{3+}). Comparing the observed 3d envelope with those previously reported for Ce^{4+} and Ce^{3+} [25, 27–30] shows that the Ce 3d spectra of the catalysts in Fig. 4, a–c, are very similar to the Ce 3d spectrum of CeO_2 (cf., e.g., the strong $3d_{3/2}$ ($4f^0$) contributions (u‴), which are missing in Ce_2O_3 [28]); therefore, the Ce is mainly of Ce^{4+} character. But in Fig. 4, b and c (i.e., after reduction as well as after reaction), the spectra also exhibit clearly visible v′ and u′ contributions, indicating that the catalysts also contain small amounts of Ce^{3+}. Thus, the surfaces of both the reduced and used samples are formed by a mixture of Ce^{4+} and Ce^{3+}, whereas the surfaces of the fresh catalysts seem to be mainly formed by Ce^{4+}. This supports the involvement of lattice oxygen in the reforming reaction.

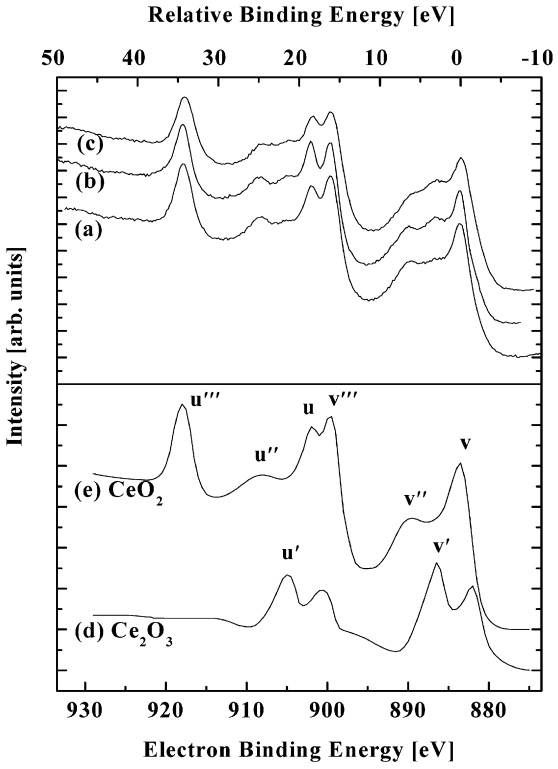

Fig. 4. Ce 3d XPS spectra for (a) as prepared $Ni_{20}Ce_{80}$, (b) reduced $Ni_{20}Ce_{80}$ (after 2 h reduction of sample (a)), and (c) tested $Ni_{20}Ce_{80}$ (after 2 h reaction of sample (a)). The spectra for Ce_2O_3 (d) and CeO_2 (e) are taken from Ref. [28], the original data were published in Ref. [27].

From XPS analysis, as a surface-sensitive technique (with a probing depth of about 1–2 nm), the distributions of Ce and Ni seem to be not homogeneous within the catalyst, at least within an area of a few atomic layers. Because of the nearly vanishing Ni intensities (not shown), the probed surface area of a single grain must be strongly enriched with Ce, or the inner core of the grain must be enriched with Ni.

A slow but continuous deactivation during the reaction and dramatic loss of catalytic activity after hydrogen treatment were observed for the $Ni_{10}Ce_{90}$ catalyst. On BET measurements, the surface area of $Ni_{10}Ce_{90}$ showed no obvious change (within experimental error) after 10 h of reaction (a decrease from 36.9 to 35.2 $m^2\,g^{-1}$) or 2 h of reduction (an increase from 36.9 to 38.2 $m^2\,g^{-1}$), indicating that no sintering effect occurs under our conditions. For the used or reduced $Ni_{10}Ce_{90}$ catalyst, XRD patterns of oxidized nickel and metallic nickel were still very weak compared to those of the fresh catalyst (see Fig. 3). This does not support significant Ni phase sintering as potential cause of catalyst deactivation. Moreover, XRD characterization (Fig. 3) and TPO study (Table 1) of tested $Ni_{10}Ce_{90}$ exhibited

Table 2
Conditions of pulse experiments[a]

Catalyst	m_{cat} (mg)	Pulse sequence	Pulse No.
Empty	0	CH_4–CO_2	15–15
CeO_2	100	CH_4–CO_2	15–15
	100	H_2–CH_4–CO_2	8–8–7
NiO	20	CH_4–CO_2	15–15
	20	H_2–CH_4–CO_2	15–19–15
	4.60	H_2–CH_4–CO_2	15–15–15
$Ni_{10}Ce_{90}$	100	CH_4–CO_2–CH_4	20–20–20
	100	H_2–CH_4–CO_2	15–15–15

[a] Operating conditions: $T = 600\,^{\circ}C$; $p = 1$ bar; Ar flow 30 ml min^{-1}; pulse volume 100 µl (4.07 µmol).

negligible coke formation. Therefore, the deactivation observed during the reaction or reduction is more likely due to a loss of active sites. Because the XRD reflections corresponding to the Ni phase of the $Ni_{10}Ce_{90}$ catalyst were very weak, together with line broadening due to its very small particles of high dispersion or the formation of Ni–Ce solid solution, the oxidation state of nickel could not be determined from the XRD measurement alone. From XPS analysis, the mixture of Ce^{4+} and Ce^{3+} was identified in the surface of both reduced and tested Ni–Ce mixed oxide, but the valance state of nickel was unclear due to its very weak intensities. To shed more light on the species of active site, we carried out a series of pulse experiments, as reported next.

3.4. Pulse experiments

3.4.1. General

Pulse experiments have been useful tools in mechanistic studies of methane dry reforming on prereduced Pt/ZrO_2 [31,32], Pt/Al_2O_3 [32], Pd/CeO_2 [33], Pd/ZrO_2 [33], Rh/Al_2O_3 [34], and fresh CeO_2 [35] catalysts. In preliminary studies on the $Ni_{10}Ce_{90}$ catalyst, in situ oxidation at 600 °C for 2 h resulted in an instable material, with mass spectrometry response signals of nitrogen and oxygen stabilizing only after about 7 h of stationary experiment. Because no difference in activity between in situ air or Ar pretreatment at 600 °C was found in 10-h reaction tests (data not shown), all samples were treated in flowing Ar for 150 min before pulse experiments. Thus, in the CH_4 or H_2 pulsed experiments, the catalyst itself was the sole source of oxygen. Among the products (i.e., H_2, H_2O, CO, and CO_2), a detection time of 5 min was not sufficient for H_2O, due to interaction with the walls of the capillary connecting the reactor with the QMS. Therefore, the amount of water released was determined indirectly based on the amount of educt pulses consumed. A blank reaction test without catalyst confirmed that the reactor itself was not catalytically active. The formation of trace amounts of products during the blank tests (<0.5% of that during the blank test of the product gases) is attributed to thermal reaction and registered as background. The conditions of pulse experiments are summarized in Table 2. The carbon balance was determined by [(the sum amount of CO and CO_2 produced)/(the amount of CH_4 consumed)] for CH_4 pulses and [(the amount of CO produced)/(the amount of CO_2 consumed)] for CO_2 pulses.

Table 3
The amount of oxygen consumed during the pulse experiments

Catalyst	m_{cat} (mg)	Theor. oxygen amount ($\times 10^{-5}$ mol)[a]	Consumed oxygen amount for complete oxidation of the reducing agent ($\times 10^{-5}$ mol)[b]		Pulse No.
			H_2–CH_4	Sum	
NiO	20	26.8	6.1 8.7	14.8	15–19
	4.60	6.2	5.6 0.9	6.4	15–15
$Ni_{10}Ce_{90}$	100	6.2	6.5	6.5	0–20
	100	6.2	5.7 0.9	6.6	15–15

[a] The amount of oxygen contained in Ni–O is calculated on the basis of the catalysts weight.

[b] The amount of consumed oxygen for complete oxidation is calculated on the basis of the hydrogen consumption for H_2 pulses and the CO_2 production for CH_4 pulses.

3.4.2. Cerium oxide

Application of CH_4 or CO_2 pulses to 100 mg ceria produced no detectable product formation exceeding background. Attempts to activate the ceria by H_2 pulses also failed. This indicates a negligible interaction of ceria with CH_4, CO_2, or H_2 at 600 °C, which is in perfect agreement with literature data. The oxidation of CH_4 by CeO_2 becomes thermodynamically viable only at temperatures above 650 °C [35], and the reduction peak of pure CeO_2 in the H_2-TPR profile is observed at about 830 °C [26]).

3.4.3. Nickel oxide

An experiment involving application of 15 CH_4 pulses followed by 15 CO_2 pulses on 20 mg of nickel oxide again revealed no detectable catalytic activity, whereas 15 pulses of H_2 over the NiO resulted in quantitative conversion. This indicates that hydrogen is a stronger reducing agent for NiO than methane. The amount of oxide oxygen calculated in 20 mg NiO was 26.8×10^{-5} mol, and the amount of oxygen consumed by the H_2 pulses was 6.1×10^{-5} mol for quantitative conversions of the reducing agent, as summarized in Table 3. Rodriguez et al. [36] evaluated the mechanism of NiO reduction by hydrogen and found that crystalline or powdered forms of NiO are directly reduced to metallic nickel at 400–460 °C without detectable formation of intermediate phases. When the partly reduced NiO was exposed to additional 19 pulses of CH_4, H_2O and CO_2 were produced with no decrease in activity and negligible formation of H_2 and CO, consuming another 8.7×10^{-5} mol of the remaining oxygen in the NiO. When an additional 15 CO_2 pulses were subsequently applied to this reduced Ni^0/NiO, no products were detectable, implying that the partially reduced nickel oxide cannot dissociate CO_2 for complete or partial reoxidation.

The experiment was repeated with only 4.6 mg of NiO, corresponding to the amount of nickel oxide in 100 mg of $Ni_{10}Ce_{90}$. The amount of oxide oxygen calculated in 4.6 mg of NiO was 6.2×10^{-5} mol. Fig. 5 gives the amounts of products during the experiment of consecutive 15 H_2–15 CH_4–15 CO_2 pulses. In Fig. 5, the amount of water released is determined indirectly by the amount of H_2 consumed in panel A and by [(the amount of CH_4 consumed) − 0.5 × (the amount of H_2 produced)] × 2 in panel B.

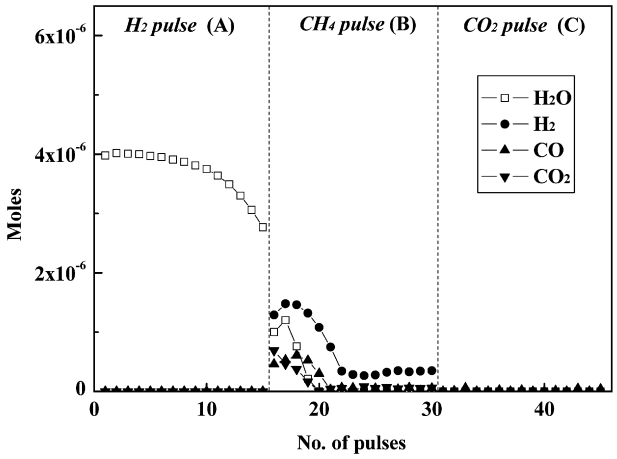

Fig. 5. The amount of products from 15 consecutive pulses of (A) H_2, (B) CH_4, and (C) CO_2 over 4.60 mg NiO. The amount of H_2O is determined indirectly by the amount of H_2 consumed in panel A and by [(the amount of CH_4 consumed) − 0.5 × (the amount of H_2 produced)] × 2 in panel B. Operating conditions: $T = 600\,^{\circ}C$; $p = 1$ bar; Ar flow 30 ml min^{-1}; pulse volume 100 µl (4.07 µmol).

With the prereduced NiO, H_2 conversion began to decrease after four pulses (see Fig. 5A), indicating that most, but not all, NiO was reduced. An estimated 5.6×10^{-5} mol of oxygen was consumed by the 15 H_2 pulses, corresponding to approximately 90% of the oxygen content of the NiO. When the 15 CH_4 pulses were applied to this highly reduced NiO, only the first 5 CH_4 pulses produced small amounts of H_2O and CO_2 apart from H_2 and CO, all of which then rapidly declined (see Fig. 5B). The formation of H_2O and CO_2 is attributed to the complete oxidation of methane with the oxygen remaining in NiO, as described in the study of 20 mg of NiO. The sum amount of oxygen consumption for the formation of H_2O and CO_2 in Figs. 5A and 5B is 6.4×10^{-5} mol, as summarized in Table 3. H_2/CO ratios were about 3 until pulse 5. A H_2/CO ratio above 2 indicates carbon formation on the catalyst surface. After pulse 6, hydrogen remained the only significant product. Apparently, the remaining oxygen in the NiO was consumed by the first five methane pulses, and methane decomposition dominated on the reduced nickel to generate carbon and H_2. When the experiment was continued with CO_2 pulses, no product was detectable (see Fig. 5C). This proves that the carbon on metallic nickel derived from methane decomposition does not react with CO_2 from the gas phase, further confirming that the metallic nickel is incapable of dissociating CO_2 for reoxidation of Ni under these conditions. No interaction between the carbon on metallic nickel and gas-phase CO_2 can explain the formation of nonremovable carbon on Ni/Al_2O_3 shown in Fig. 2d and Table 1. This is quite different from the result with prereduced Rh/Al_2O_3, where most of the surface carbon on Rh is successfully oxidized to CO by CO_2 from the gas phase [34].

3.4.4. $Ni_{10}Ce_{90}$ mixed oxide

The products from consecutive 20 CH_4–20 CO_2–20 CH_4 pulses on 100 mg of $Ni_{10}Ce_{90}$ at 600 °C are depicted in Fig. 6. In Fig. 6a, again the amount of H_2O is determined indirectly by [(the amount of CH_4 consumed) − 0.5 × (the amount of H_2 produced)] × 2. When the first eight CH_4 pulses were introduced to $Ni_{10}Ce_{90}$, H_2O, and CO_2 were the main products. H_2O/CO_2 ratios of about 2 and carbon balances of unity were found (see panel A of Fig. 6b), implying that the complete oxidation of methane occurred without carbon formation. Furthermore, there seems to be a formation period, because the highest activity is reached not until five pulses. Because this catalyst was not reduced, the question of where this reaction occurs can then be asked. Neither NiO nor CeO_2 activates CH_4, as shown previously. Therefore, it is assumed that the interfacial oxygen in the Ni–Ce boundary (Ni–O–Ce site) is the active component for the complete oxidation of methane. This is not unreasonable, because several studies point to the formation of M–O–Ce surface complexes with metals such as Pd, Pt, Rh, and Au at the interface [7,37–39]. As summarized in Table 3, 6.5×10^{-5} mol of oxygen is consumed by total methane oxidation on $Ni_{10}Ce_{90}$, which corresponds to about the total oxygen content of the Ni–oxygen in the catalyst. Moreover, for the $Ni_{20}Ce_{80}$ mixed

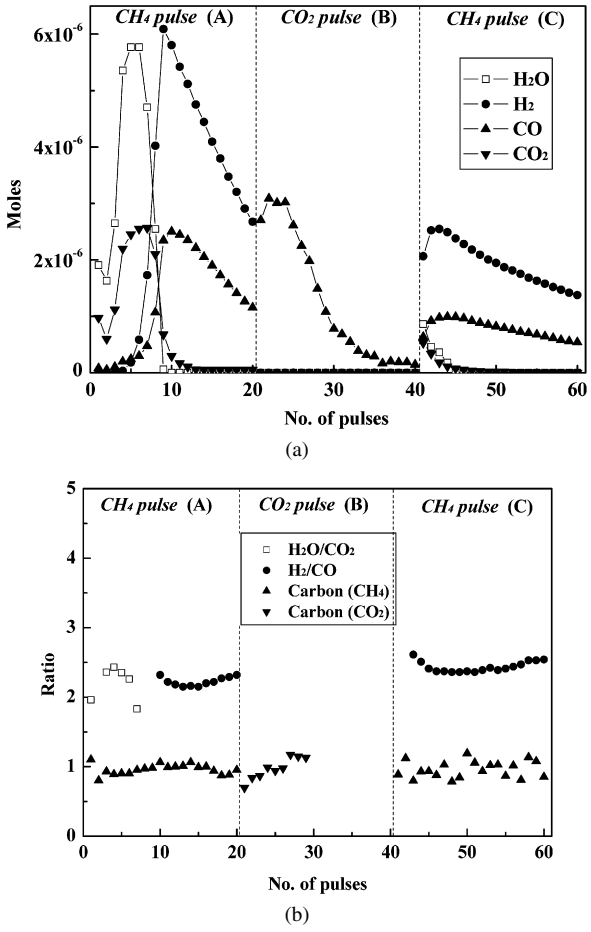

Fig. 6. (a) The amount of products from 20 consecutive pulses of (A) CH_4, (B) CO_2, and (C) CH_4 over 100 mg $Ni_{10}Ce_{90}$. (b) The ratio of (■) H_2O/CO_2, (●) H_2/CO, (▲) carbon determined by [(the sum amount of CO and CO_2 produced)/(the amount of CH_4 consumed)] for CH_4 pulses, and (▼) carbon determined by [(the amount of CO produced)/(the amount of CO_2 consumed)] for CO_2 pulses. The amount of H_2O is determined indirectly by [(the amount of CH_4 consumed) − 0.5 × (the amount of H_2 produced)] × 2. Operating conditions: $T = 600\,^{\circ}C$; $p = 1$ bar; Ar flow 30 ml min^{-1}; pulse volume 100 µl (4.07 µmol).

oxide, the amount of oxygen consumed by total methane oxidation (15.5×10^{-5} mol) is increased by factor of 2.3 relative to $Ni_{10}Ce_{90}$ [24].

After the eighth pulse, CO_2 and H_2O formation ceased, and the product was dominated by H_2 and CO, the formation of the latter also continuously decreased during the following pulses. Here the oxygen consumed must originate from the ceria lattice. It is believed that storage oxygen in the ceria is provided to the active Ni–Ce sites, which are now depleted of the original oxygen, leading to the creation of oxygen vacancies in the ceria. The amount of syngas formed is conceivably based on the diffusion rate of lattice oxygen correlated to oxygen concentration gradient. The H_2/CO ratios produced remained close to 2, and carbon balances were about unity (see panel A of Fig. 6b). Therefore, no indication for carbon deposition was found on the $Ni_{10}Ce_{90}$ by CH_4 pulses.

When the catalyst was subjected to CO_2 pulses, CO_2 was converted exclusively into equivalent of CO, as shown in Figs. 6aB and 6bB. The total amount of CO obtained from CO_2 during the 20 pulses was 2.51×10^{-5} mol. Because CO_2 pulses resulted no activity with the as-prepared $Ni_{10}Ce_{90}$ (not shown) or with reduced nickel (see Fig. 5c), the CO formation indicates either that reduced Ni–Ce sites are reoxidized or that the ceria oxygen vacancies created during the methane pulses 8–20 are supplemented by CO_2 dissociation and vacancy filling. The subsequent 20 CH_4 pulses (see below) seem to indicate that the CO formation arises from reoxidation of the ceria oxygen vacancies. Compared with the total amount of CO released from the CH_4 pulses in panel A (2.55×10^{-5} mol), the oxygen vacancies are fully replenished by CO_2 dissociation. Comparing the CO production rate of the two processes (creation and recovery of oxygen vacancies) in Fig. 6a demonstrates that the supplementation of oxygen vacancies in panel B is clearly faster than their generation in panel A, indicating that the oxygen vacancies react very rapidly with CO_2 to allow ready replenishment.

The interaction of hydrogen with cerium-based oxides has been widely studied, and ceria is known to be able to store hydrogen [25,40]. Therefore, the CO formation could have originated from the RWGS reaction between hydrogen stored in the ceria and subsequent CO_2 pulses. However, this effect was negligible here for two reasons. First, if hydrogen storage occurred during the methane pulses, then the H_2/CO ratios produced should be <2, due to the additional consumption of H_2. At the same time, H_2O should be detectable. However, the H_2/CO ratios produced remained close to 2, and the amount of H_2O released was negligible after the 9th methane pulse. Second, if the RWGS reaction occurred during the CO_2 pulses, then H_2O as well as CO should be produced. However, as shown in panel B of Fig. 6a, CO was the only product produced when CO_2 pulses were applied.

The subsequent 20 CH_4 pulses produced essentially H_2 and CO, with only trace amounts of H_2O and CO_2. The amounts of H_2O and CO_2 released in Fig. 6aC are significantly lower than those shown in Fig. 6aA. Because regeneration of the Ni–O–Ce sites should have led to total oxidation, this supports the view

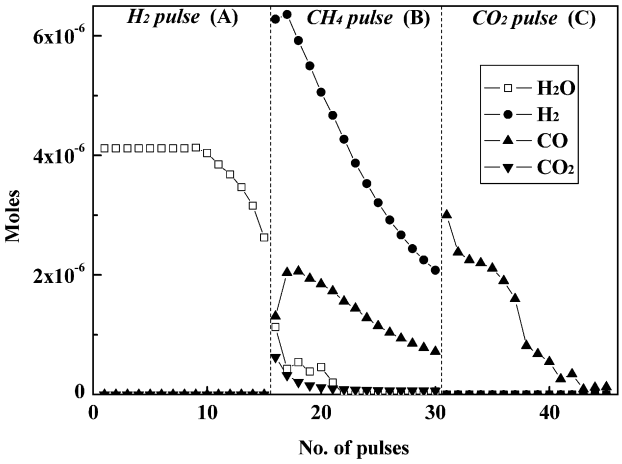

Fig. 7. The amount of products from 15 consecutive pulses of (A) H_2, (B) CH_4, and (C) CO_2 over 100 mg $Ni_{10}Ce_{90}$. The amount of H_2O is determined indirectly by the amount of H_2 consumed in panel A and by [(the amount of CH_4 consumed) $- 0.5 \times$ (the amount of H_2 produced)] $\times 2$ in panel B. Operating conditions: $T = 600\,^{\circ}C$; $p = 1$ bar; Ar flow 30 ml min^{-1}; pulse volume 100 μl (4.07 μmol).

that the oxygen used for the initial formation of H_2O and CO_2 were not regenerated, and only ceria oxygen vacancies were reoxidized by the CO_2 treatment. CO_2 dissociation apparently allows recharging of the oxygen vacancies in the ceria lattice, but not direct recharging of the consumed interfacial oxygen of the Ni–Ce boundary. H_2/CO ratios were about 2, but increased slightly compared with those of the first 20 CH_4 pulses.

After the full supplementation of oxygen vacancies by CO_2 dissociation, the deactivation for syngas production slowed, but the amount of H_2 and CO released decreased significantly (compare Figs. 6aA and 6aC). This might be due to microstructural changes during the depletion of reactive oxygen by the subsequent methane pulses.

Another series of pulse experiments was conducted, starting with H_2 pulses. The results of the 15 H_2–15 CH_4–15 CO_2 pulses on 100 mg of $Ni_{10}Ce_{90}$ are shown in Fig. 7. Although the first 10 pulses of hydrogen were completely converted, conversion dropped over the subsequent 5 pulses. Total oxygen consumption was 5.7×10^{-5} mol. During the next 15 CH_4 pulses, the small amount of CO_2 initially formed corresponds to the 0.9×10^{-5} mol of oxygen remaining in the NiO. The sum amount of oxygen consumption for the formation of H_2O and CO_2 shown in Figs. 7A and 7B is 6.6×10^{-5} mol—very close to the total oxygen content of the NiO in the catalyst, as summarized in Table 3. In panel B, the product is dominated by H_2 and CO formation in amounts comparable to those formed during the CH_4 pulses in Fig. 6a. Considering the total amount of oxygen consumption for the complete oxidation of methane in Fig. 6a (6.5×10^{-5} mol), the similar behavior and amount of production seem reasonable because of its generation on similar amounts of the active Ni–Ce sites. When the 15 CO_2 pulses were applied to $Ni_{10}Ce_{90}$, CO_2 was converted exclusively again to CO. The sum amount of CO obtained was 2.01×10^{-5} mol. Compared with the sum amount of CO released by CH_4 (2.07×10^{-5} mol), the ceria oxygen

vacancies were completely replenished again by CO_2 dissociation.

3.5. Suggested mechanism

Based on the results of this investigation, the interfacial oxygen in the Ni–Ce boundary of the $Ni_{10}Ce_{90}$ catalyst seems to be an active component for the complete oxidation of methane, because (i) nickel oxide or cerium oxide itself shows no activity with methane, (ii) the amount of oxygen consumed by the total oxidation of methane on $Ni_{10}Ce_{90}$ is close to the total oxygen content of the Ni-oxygen in the catalyst (see Table 3), and (iii) for $Ni_{20}Ce_{80}$, the amount of oxygen consumed by the complete oxidation of methane increases by factor of 2.3 compared with $Ni_{10}Ce_{90}$. Therefore, the first 1 mol CH_4 is converted to 2 mol H_2O and 1 mol CO_2 at the Ni–Ce boundary accompanying the consumption of the interfacial oxygen (Fig. 6, pulses 1–8). The resulting site is considered the active site for the reforming reaction, where subsequently 1 mol CH_4 is reformed through the reaction with the oxygen migrated from ceria lattice to release 2 mol H_2 and 1 mol CO. The reaction is concomitant with the creation of oxygen vacancies of the ceria lattice. Thereafter, the oxygen vacancies are supplemented by oxygen arising from the dissociative adsorption of 1 mol CO_2 to produce 1 mol CO. However, the consumed interfacial oxygen in the Ni–Ce boundary cannot be recovered by CO_2 dissociation.

Based on these suggestions, the origin of unusual $Ni_{10}Ce_{90}$ mixed-oxide properties for the CO_2 reforming of methane can be discussed. First, the catalytic property in the absence of a prereduction step relies on the reactivity of oxygen contained in the Ni species. The immediate activity of $Ni_{10}Ce_{90}$ is based on the active interfacial oxygen in the Ni–Ce boundary (Ni–O–Ce site), which leads to the complete oxidation of methane and the creation of active sites for the subsequent reforming reaction, whereas the strong interaction of the $NiAl_2O_4$ spinel retards the activity of Ni/Al_2O_3. Second, the coking resistance relies on the reactivity of lattice oxygen in the catalyst support. The ceria lattice oxygen, with high mobility, participates in the reforming reaction through migration, leading to the formation of CO and oxygen vacancies of ceria lattice. On the other hand, the lack of interaction between the surface carbon on metallic nickel and lattice oxygen of γ-Al_2O_3 results in the formation of nonremovable carbon on the Ni/Al_2O_3 catalyst. Finally, based on the negligible amount of surface area loss and coke formation during reaction, the continuous deactivation behavior of $Ni_{10}Ce_{90}$ is due mainly to a loss of active sites. In the pulse experiment on $Ni_{10}Ce_{90}$, the continued consumption of reactive oxygen in the condition of no supplementation or delayed replenishment resulted in deactivation. Thus, in the CO_2 reforming of methane a balanced rate between the generation and supplement of oxygen vacancies seems to be needed to avoid deactivation.

4. Conclusions

In this study, the origin of the exceptional $Ni_{10}Ce_{90}$ mixed-oxide properties relative to the Ni/Al_2O_3 catalyst (i.e., immediate activation in the absence of catalyst prereduction, no tendency toward coking, and high catalytic activity) and its slow deactivation for the CO_2 reforming of methane was explored and understood at a fundamental level by XRD, XPS, pulse experiments and regeneration tests. Based on the results, a reaction mechanism was suggested.

Several conclusions can be drawn from this investigation:

1. The catalytic property with no prereduction step relies on the reactivity of oxygen contained in the Ni phase. Active interfacial oxygen in the Ni–Ce boundary leads to a rapid startup operation of $Ni_{10}Ce_{90}$, whereas slow decomposition of $NiAl_2O_4$ spinel results in the long induction period of the Ni/Al_2O_3 catalyst.
2. Coking resistance and catalytic activity rely on the reactivity of lattice oxygen in the Ni-catalyst support. The ceria lattice oxygen participates in the reforming reaction through migration, leading to the formation of oxygen vacancies in the ceria lattice. Subsequently, the vacancies are completely supplemented by oxygen arising from CO_2 dissociation.
3. The stability of $Ni_{10}Ce_{90}$ relies on the balance between the rate of generation and supplement of oxygen vacancies. Unbalanced rates of these processes result in deactivation.

Acknowledgments

Financial support was provided by the Deutsche Forschungsgemeinschaft (grant GRK 232). The authors thank H. Höltzen for assisting with product analysis, R. Richter for constructing the reactor, R. Haberkorn for performing XRD studies, and R. Nagel for helping with the BET measurements.

References

[1] www.fuelcells.umicore.com/de/downloads/fcprotonics032004.pdf.
[2] J.A.C. Dias, J.M. Assaf, J. Power Sources 139 (2005) 176.
[3] D.K. Kim, W.F. Maier, J. Catal. 238 (2006) 142.
[4] J. Scheidtmann, P.-A.W. Weiss, W.F. Maier, Appl. Catal. A 222 (2001) 79.
[5] http://en.wikipedia.org/wiki/Rare_earth_element.
[6] C.T. Campbell, C.H.F. Peden, Science 309 (2005) 713.
[7] A. Trovarelli, Catal. Rev. Sci. Eng. 38 (1996) 439.
[8] J. Kaŝpar, P. Fornasiero, M. Graziani, Catal. Today 50 (1999) 285.
[9] E. Rocchini, A. Trovarelli, J. Llorca, G.W. Graham, W.H. Weber, M. Maciejewski, A. Baiker, J. Catal. 194 (2000) 461.
[10] F. Esch, S. Fabris, L. Zhou, T. Montini, C. Africh, P. Fornasiero, G. Comelli, R. Rosei, Science 309 (2005) 752.
[11] Y. Li, Q. Fu, M. Flytzani-Stephanopoulos, Appl. Catal. B 27 (2000) 179.
[12] P. Bera, K.C. Patil, V. Jayaram, G.N. Subbanna, M.S. Hegde, J. Catal. 196 (2000) 293.
[13] J. Barrault, A. Alouche, V. Paulboncour, L. Hilaire, A. Percheronguegan, Appl. Catal. 46 (1989) 269.
[14] S. Park, R.J. Gorte, J.M. Vohs, Appl. Catal. A 200 (2000) 55.
[15] X. Wang, R.J. Gorte, Appl. Catal. A 224 (2002) 209.
[16] TOPAS, Version 2.1, Bruker AXS, Karlsruhe.
[17] R.W. Cheary, A.A. Coelho, J. Appl. Crystallogr. 25 (1992) 109.
[18] equiTherm, Version 3.02, Scienceware/VCH, 1997.
[19] S. Wang, G.Q. Lu, Appl. Catal. B 19 (1998) 267.
[20] Z. Xu, Y. Li, J. Zhang, L. Chang, R. Zhou, Z. Duan, Appl. Catal. A 210 (2001) 45.
[21] J.M. Rynkowski, T. Paryjczak, M. Lenik, M. Farbotko, J. Goralski, J. Chem. Soc. Faraday Trans. 91 (1995) 3481.
[22] S. Klein, S. Thorimbert, W.F. Maier, J. Catal. 163 (1996) 476.

[23] M. Stöckmann, F. Konietzni, J.U. Notheis, J. Voss, W. Keune, W.F. Maier, Appl. Catal. A 208 (2001) 343.
[24] D.K. Kim, Ph.D. thesis, Universität des Saarlandes, 2006.
[25] G. Wrobel, M.P. Sohier, A. D'Huysser, J.P. Bonnelle, Appl. Catal. A 101 (1993) 73.
[26] N. Yisup, Y. Cao, W.-L. Feng, W.-L. Dai, K.-N. Fan, Catal. Lett. 99 (2005) 207.
[27] J.W. Allen, J. Magn. Magn. Mater. 47–48 (1985) 168.
[28] K. Gschneider, L. Eyring, S. Hüfner, Handbook on the Physics and Chemistry of Rare Earths, vol. 10, North-Holland, Amsterdam, 1987.
[29] F.B. Noronha, E.C. Fendley, R.R. Soares, W.E. Alvarez, D.E. Resasco, Chem. Eng. J. 82 (2001) 21.
[30] D.H. Kim, S.I. Woo, Catal. Lett. 98 (2004) 23.
[31] S.M. Stagg, F.B. Noronha, G. Fendley, D.E. Resasco, J. Catal. 194 (2000) 240.
[32] J.H. Bitter, K. Seshan, J.A. Lercher, J. Catal. 176 (1998) 93.
[33] S. Sharma, S. Hilaire, J.M. Vohs, R.J. Gorte, H.-W. Jen, J. Catal. 190 (2000) 199.
[34] M.F. Mark, W.F. Maier, Angew. Chem. Int. Ed. 33 (1994) 1657.
[35] K. Otsuka, Y. Wang, E. Sunada, I. Yamanaka, J. Catal. 175 (1998) 152.
[36] J.A. Rodriguez, J.C. Hanson, A. Frenkel, J.-Y. Kim, M. Perez, J. Am. Chem. Soc. 124 (2002) 346.
[37] J.Z. Shyu, K. Otto, W.L.H. Watkins, G.W. Graham, R.K. Belitz, H.S. Gandhi, J. Catal. 114 (1988) 23.
[38] M.S. Brogan, T.J. Dines, J.A. Cairns, J. Chem. Soc. Faraday Trans. 90 (1994) 1461.
[39] Q. Fu, H. Saltsburg, M. Flytzani-Stephanopoulos, Science 301 (2003) 935.
[40] C. Lamonier, A. Ponchel, A. D'Huysser, L. Jalowiecki-Duhamel, Catal. Today 50 (1999) 247.